Redox Biology 84 (2025) 103693

Contents lists available at ScienceDirect

Redox Biology

journal homepage: www.elsevier.com/locate/redox

Dysregulated lipids homeostasis disrupts CHAC1-mediated ferroptosis driving fibroblast growth factor receptor tyrosine kinase inhibitor AZD4547 resistance in gastric cancer

Jingwen Chen [a,g,1], Yedi Huang [b,g,1], Daocheng Zuo [b], Ruimin Shan [b], Songmao Li [b], Ran Li [b], Dong Hua [c], Qiang Zhan [d], Xudong Song [e], Yun Chen [b,g,*], Pei Ma [a,g,**], Ling Ma [a,g,***], Guoquan Tao [f,****], Yongqian Shu [a,f,g,*****]

[a] Department of Oncology, The First Affiliated Hospital with Nanjing Medical University, Nanjing, 210029, PR China
[b] Department of Immunology, School of Basic Medical Sciences, Jiangsu Key Lab of Cancer Biomarkers, Prevention and Treatment, Nanjing Medical University, Nanjing, 210000, PR China
[c] The Affiliated Wuxi People's Hospital of Nanjing Medical University, School of Medicine, Jiangnan University, Wuxi, 214000, PR China
[d] Departments of Gastroenterology, the Affiliated Wuxi People's Hospital of Nanjing Medical University & Department of Medical Genetics, Nanjing Medical University, Nanjing, 210000, PR China
[e] Department of Gastrointestinal surgery, The Affiliated Huaian No. 1 People's Hospital of Nanjing Medical University, Huaian, 223300, PR China
[f] Gusu School, Nanjing Medical University, Suzhou, 211166, PR China
[g] Collaborative Innovation Center for Cancer Personalized Medicine, Nanjing Medical University, Nanjing, 211166, PR China

ARTICLE INFO

Keywords:
Gastric cancer
FGFR-TKI resistance
Ferroptosis
CHAC1
Cholesterol metabolism
Lipidomics

ABSTRACT

Aims: This study investigates the mechanisms underlying acquired resistance to FGFR tyrosine kinase inhibitor (FGFR-TKI) in gastric cancer (GC), focusing on the interplay between ferroptosis and lipid metabolism of tumor cells.

Methods: We constructed FGFR-TKI-resistant cell lines from GC cells. RNA sequencing was performed to identify differentially expressed genes (DEGs) related to ferroptosis and assess lipid metabolism in resistant cells. GC microenvironment lipid profile was characterized by HPLC-MS/MS lipidomics. The effects of CHAC1 and cholesterol synthesis modulation on ferroptosis and FGFR-TKI resistance were assessed using in vitro and in vivo models.

Results: We found that FGFR-TKI can induce ferroptosis in FGFR-TKI-sensitive cells, while resistant cells exhibit decreased sensitivity to ferroptosis due to reduced CHAC1 expression, a key glutathione-specific degrading enzyme. Overexpression of CHAC1 enhances FGFR-TKI cytotoxicity. Additionally, cholesterol accumulation in resistant cells, associated with diminished stearic acid (SA) uptake, confers FGFR-TKI-induced ferroptosis resistance. In vivo studies show that CHAC1 overexpression or cholesterol synthesis inhibition can reverse FGFR-TKI resistance, which is dependent on ferroptosis.

Conclusions: Dysregulated lipid homeostasis downregulated CHAC1-mediated ferroptosis, leading to FGFR-TKI resistance in gastric cancer. Overexpression of CHAC1 or inhibiting cholesterol synthesis presents promising therapeutic strategies to overcome FGFR-TKI resistance in GC.

* Corresponding author. Department of Immunology, School of Basic Medical Sciences, Jiangsu Key Lab of Cancer Biomarkers, Prevention and Treatment, Nanjing Medical University, Nanjing, 210000, PR China.
** Corresponding author. Department of Oncology, The First Affiliated Hospital with Nanjing Medical University, Nanjing, 210029, PR China.
*** Corresponding author. Department of Oncology, The First Affiliated Hospital with Nanjing Medical University, Nanjing, 210029, PR China.
**** Corresponding author.
***** Corresponding Author. Department of Oncology, The First Affiliated Hospital with Nanjing Medical University, Nanjing, 210029, PR China.
E-mail addresses: chenyun@njmu.edu.cn (Y. Chen), mapei@njmu.edu.cn (P. Ma), maling@njmu.edu.cn (L. Ma), taoguoquan5698102@163.com (G. Tao), shuyongqian@csco.org.cn (Y. Shu).
[1] Contributed equally.

https://doi.org/10.1016/j.redox.2025.103693
Received 10 February 2025; Received in revised form 17 April 2025; Accepted 19 May 2025
Available online 22 May 2025

Abbreviations

FGFR-TKI	Fibroblast growth factor receptor tyrosine kinase inhibitor
GC	Gastric cancer
DEGs	Differentially expressed genes
PCD	Programmed cell death
TME	Tumor microenvironment
FRGs	Ferroptosis-related genes
TIF	Tumor interstitial fluid
CHAC1	Gutathione-specific γ-glutamylcyclotransferase 1
ROS	Lipid reactive oxygen species
TEM	Transmission electron microscopy
As	Fatty acids
PA	Palmitoleic acid
OA	Oleic acid
AA	Arachidonic acid
SA	Stearic acid
TG	Triglyceride
FATPs	Fatty acid transport proteins
FABPs	Fatty acid-binding proteins
DAG	Diacylglycerols
PE	Phosphatidylethanolamine
PI	Phosphatidylinositol
PS	Phosphatidylserine
Cer	Ceramides
SM	Sphingomyelins
PC	Phosphatidylcholine
lysoPC	lysophosphatidylcholine
PG	Phosphatidylglycerol
HFD	High-fat diet
LDs	Lipid droplets
7-DHC	7-Dehydrocholesterol
IHC	Immunohistochemistry
HPLC-MS/MS	Ultra-High-performance liquid chromatography–mass spectrometry
GSH	Glutathione
NAC	N-Acetylcysteine

1. Introduction

Gastric cancer (GC) is the fifth most prevalent malignancy and the fourth highest cause of cancer-related mortality globally, with an expected 62 % increase in disease burden by 2040 [1]. Despite advancements in chemotherapy and targeted therapies, clinical outcomes remain suboptimal due to high molecular heterogeneity of GC, which restricts therapeutic options and drives drug resistance [2,3]. Fibroblast growth factor receptor tyrosine kinase inhibitor (FGFR-TKI) show promise for patients with gain-of-function FGFR alterations [4,5], yet resistance mechanisms remain elusive. Emerging evidence highlights enhanced antioxidant capacity as a key drug resistance driver of GC cells [6], while dysregulated lipid metabolism, a hallmark of GC progression, may synergistically interact with redox adaptations to promote resistance. Elucidating this crosstalk is critical for developing strategies to overcome FGFR-TKI resistance.

Ferroptosis, a form of programmed cell death (PCD) characterized by lipid peroxidation and redox-active iron accumulation, is recognized as a promising strategy for eliminating cancer cells [7]. Studies have shown that cancer cells, including GC cells, exhibit increased susceptibility to ferroptosis, and chemical inducers have been demonstrated to effectively suppress tumor growth [8,9]. Ferroptosis is also implicated in the response of cancer cells to a range of therapeutic agents, and its dysregulation may lead to chemotherapy resistance and treatment failure [10,11]. Nevertheless, the relationship between ferroptosis and FGFR-TKI resistance merits further exploration.

Lipid metabolism, particularly cholesterol homeostasis, is increasingly recognized as a pivotal factor in cancer progression and response to therapy [12,13]. Disruptions in lipid homeostasis can reshape the tumor microenvironment (TME), potentially leading to therapeutic resistance [14,15]. Moreover, lipid metabolism directly regulates the onset and sensitivity of ferroptosis by controlling the types and levels of specific fatty acids (FAs) and the activity of related enzymes [16,17]. Therefore, lipidomics in GC, especially concerning FGFR-TKI resistance, is a burgeoning field with potential for the discovery of novel biomarkers and therapeutic targets.

In this study, we aimed to investigate the mechanisms of acquired resistance to FGFR-TKI in GC, with a particular focus on the interplay between ferroptosis and lipid metabolism. We hypothesized that disruptions in lipid homeostasis, specifically cholesterol metabolism and fatty acid uptake, may contribute to the development of FGFR-TKI resistance in GC cells. Furthermore, we assessed the therapeutic potential of targeting CHAC1, a glutathione-specific degrading enzyme, and cholesterol synthesis as novel strategies to reverse FGFR-TKI resistance.

2. Experimental section

2.1. Cell lines and culture Conditions

Two gastric adenocarcinoma FGFR-TKI-resistant cell lines BGC823-R and MGC803-R were generated from BGC-823 and MGC-803 cells, which were characterized by high FGFR1 expression and initial sensitivity to FGFR-TKI. These resistant cell lines were established by treating with 1 μM AZD4547 (a representative FGFR-TKI) for 72–96 h, followed by continuous selection over 5–6 growth cycles. FGF2 (Peprotech, #100-18B) was added to the culture medium to activate FGFR1. In vitro experiments involved treating the cells with the following compounds: AZD4547 (Selleck, #S2801), Erastin (Cayman Chemical, #17754), RSL3 (Cayman Chemical, #19288), Ferrostatin-1 (Fer-1, Cayman Chemica, #17729), N-Acetylcysteine (NAC, MCE, #HY-B0215), L-Glutathione reduced (GSH, MCE, #HY-D0187), Cholesterol (MCE, #HY-N0322A), palmitoleic acid (PA, Cayman Chemical, #10009871), oleic acid (OA, Cayman Chemical, #90260), arachidonic acid (AA, Cayman Chemical, #90010), stearic acid (SA, Cayman Chemical, #10011298), Lovastatin (Selleck, #S2061). All the tumor cell lines were cultured in Dulbecco's modified Eagle's medium (DMEM, Gibco, #C11995500BT) with 10 % fetal bovine serum (Newzerum, #FBS-CS500) and 1 % penicillin-streptomycin (Gibco, #15140-122) at 37 °C in the presence of 5 % CO2.

2.2. RNA sequencing and bioinformatic analysis

RNA sample preparation and RNA sequencing methodologies were previously described in our study [18]. Heat maps and volcano plots showed DEGs of FGFR-TKI-sensitive and resistant cells. Kyoto Encyclopedia of Genes and Genomes (KEGG) and Gene ontology (GO) analyses were used to identify the correlation between ferroptosis and DEGs. The list of ferroptosis-related genes (FRGs) is available through the FerrDb Database (http://www.zhounan.org/ferrdb).

2.3. Plasmids or siRNA transfection and lentivirus infection

All plasmids and lentivirus constructs were developed by Genechem (Shanghai, China). Cells were seeded in 6-well plates at 3-5 × 10^5 cells/well and transfected with 3 μg CHAC1-overexpressing plasmid or 50 nM siRNA targeting human CHAC1 (sequences in Supplementary Table S1) using 5 μL Lipofectamine 3000 (Invitrogen, #L3000015) in 250 μL Opti-

MEM (Gibco, #31985070). After 6-h incubation, the medium was replaced with fresh DMEM (Gibco, #C11995500BT). For lentiviral infection, MGC803-R and BGC823-R cells were treated with CHAC1-overexpressing lentivirus or control virus in the presence of 5 μg/mL Polybrene (Beyotime, #C0351) for 16 h. To select stably transduced cells, puromycin (MCE, #HY-K1057) was added at 2 μg/mL for 7 days. Surviving cells were expanded for subsequent experiments.

2.4. Cell proliferation and death assay

Cell proliferation was assessed using CCK8 (Sigma-Aldrich, #96992) assay or flow cytometry with Propidium Iodide (PI, Beyotime, #ST512) staining. For the CCK8 assay, 5×10^3 tumor cells were seeded in 96-well plates with 200 μL culture medium and allowed to adhere overnight. Then cells were treated with gradient concentrations of AZD4547, RSL3, erastin or indicated lipids (50 μM SA, AA, OA or PA) at the indicated concentrations for 36 or 72 h. Following treatment, cells were incubated with CCK8 in a serum-containing medium for 1 h before measuring absorbance at OD450 nm using a plate reader (Biotek Synergy). For cell death analysis, 2×10^5 tumor cells were seeded in 6-well plates with 2 mL culture medium and allowed to adhere overnight. After treatment, cells were stained with 2 μg/mL PI (final concentration) from a 1 mg/mL stock and incubated with cells for 15 min at 37 °C in the dark prior to flow cytometry analysis (BD, FACSCalibur). Data were analyzed using FlowJo V10.6. software.

2.5. Colony formation, migration and invasion assay

For the colony formation assay, 1.5×10^3 siRNA or plasmid-transfected cells were treated with 1 μM AZD4547 or DMSO for 10–14 d after adherence, then fixed, stained with crystal violet, and colonies >50 cells were counted using ImageJ software. For migration, wound healing assays involved scratching confluent monolayers treated with 1 μM AZD4547 or DMSO, capturing images at 0 and 24 h, and analyzing the distance migrated. For transwell invasion assays, 5×10^4 cells were seeded in the upper chamber of matrigel-coated transwell plates, with 10 % FBS in the lower chamber to attract the cells. After 24 h, cells that invaded through the Matrigel were fixed, stained with crystal violet, and counted under a microscope. The data shown were representatives of 3 independent experiments.

2.6. Lipid peroxidation and glutathione assay

To assess lipid peroxidation, 3-5 $\times 10^3$ cells were seeded in 96-well plates and treated with or without AZD4547 (1 μM or 2.5 μM) or RSL3 (2 μM) or erastin (2.5 μM or 5 μM) for 48h, and then subsequently incubated with either 5 μM BODIPY-581/591 C11 (Invitrogen, #D3861) or 10 μM DCFH-DA (Beyotime, #S0033S). For fluorescence imaging, the above cells were counterstained with Hoechst 33342; and then visualized under a fluorescence microscope to calculate the relative lipid ROS index (relative lipid ROS index = oxidized C11/non-oxidized C11). Flow cytometry measured fluorescence intensity after staining with BODIPY-581/591 C11 or DCFH-DA using a flow cytometer (BD, FACSCalibur). For glutathione measurement, a Glutathione Assay Kit (Sigma-Aldrich, #CS0260) was used following the manufacturer's instructions. In brief, 2×10^5 cells were seeded in 6-well plates and treated with or without 1 μM AZD4547 treatment for 48h, and then lysed and centrifuged. The supernatant was assayed in a microplate reader for kinetic monitoring at ΔA412/min. Total glutathione content was calculated based on the standard curve and sample weight.

2.7. Transmission electron microscopy

Adherent GC cells treated with DMSO, AZD4547 (2.5 μM) or RSL3 (2 μM) for 48h were harvested using cell scrapers, centrifuged at 1500 rpm for 10 min, and fixed with 2.5 % glutaraldehyde. Ultrathin sections (80 nm) were prepared and examined using a transmission Electron Microscope (JEOL, JEM-1400Flash).

2.8. RNA Isolation and qRT-PCR analysis

Gastric cancer cells treated with AZD4547, fatty acids (SA, PA, OA, AA) or lovastatin were rinsed with prechilled PBS (Gibco, #C10010500BT) and lysed in Trizol reagent (Ambion, #15596018). Total RNA was extracted using Cell/Tissue Total RNA Isolation Kits (Vazyme Biotech, RC112-01) and quantified with a NanoDrop Spectrophotometer (Onedrop). gDNA removal and cDNA synthesis (Vazyme Biotech, #R323) and qRT-PCR (Vazyme, #Q511-02/03) were performed using Applied Biosystems SimpliAmp Thermal Cycler (Thermo Fisher Scientific) and ABI StepOnePlus (Life technologies) respectively. Relative gene expression was normalized to β-actin expression and calculated using the $2^{-\Delta\Delta Ct}$ method. Primer sequences are listed in Supplementary Table S2.

2.9. Protein extraction and Western blotting

Protein was extracted from cells using RIPA Lysis Buffer (Beyotime, #P0013C) and Protease Inhibitor Cocktail (Cell Signaling Technologies, #7012L). After the BCA protein concentrations assay (Beyotime, #P0010), samples were separated by electrophoresis using precast gels (GenScript, #M00657, #M00653) and transferred onto PVDF membranes (BIO-RAD, #1620177). After blocking with skim milk, membranes were incubated within primary antibodies at 4 °C overnight. The secondary antibody of anti-rabbit IgG or anti-mouse IgG were used at RT for 1 h. Detailed information on all antibodies, including sources, product codes, and dilution ratios, is provided in Supplementary Table S3. Blots were visualized using High-Performance Fluorescence System (Syngene) with an ECL Substrate (Tanon, #180–501).

2.10. Immunohistochemistry (IHC)

Gastric adenocarcinoma tissues and matched adjacent tissues were obtained from The First Affiliated Hospital of Nanjing Medical University with ethical approval (2018-SRFA-074). Tissues were fixed with 4 % paraformaldehyde, paraffin-embedded and sectioned. The sections were incubated with anti-CHAC1(Sigma-Aldrich, #AV42623, dilution 1:100) followed by HRP-linked anti-rabbit IgG, with hematoxylin counterstaining. Images were captured using digital microscope cameras (Olympus BX53) and CellSens software. Staining intensity was analyzed using ImageJ 2.0 software, following the methodology described previously [19].

2.11. Collection of serum and TIF from GC patients

Collection approach of serum and tumor interstitial fluid (TIF) from 19 GC patients referred to previous studies [20–22]. Peripheral blood was collected into vacuum tubes without anticoagulant, allowed to clot at RT, and then centrifuged at 3000 rpm for 5 min and 12000 rpm for 20 min at 4 °C to obtain serum. Tumor tissues, collected within 30–45 min post-surgery, were rinsed in prechilled PBS, minced (0.1–0.3 g), and eluted in PBS at 37 °C with 5 % CO_2 for 1 h. After centrifugation at 200*g* for 5 min and 4000 g for 20 min at 4 °C, TIF was collected from the supernatant. Both serum and TIF were snap-frozen in liquid nitrogen and stored at −80 °C for further analysis.

2.12. Lipidomics analysis

Lipidomics analysis of TIF and serum samples was conducted using Ultra-High-performance liquid chromatography-mass spectrometry (HPLC-MS/MS) by Novogene Co., Ltd. (Beijing, China). The Vanquish UHPLC system (ThermoFisher) coupled with an Orbitrap Q ExactiveTM HF mass spectrometer (ThermoFisher) was utilized for lipid metabolite

extraction and identification with Lipidmaps and Lipidblast databases. Data analysis included principal components analysis (PCA) and partial least squares discriminant analysis (PLS-DA) via metaX software. Metabolites with VIP >1 and P value < 0.05 and fold change≥ 2 or FC ≤ 0.5 were defined to be differential lipid metabolites. Volcano plots and heat maps were generated in R using ggplot2 and Pheatmap, with data normalized to z-scores.

2.13. Cholesterol content and neutral lipid content assay

Cellular cholesterol content and neutral lipid content were assessed in FGFR-TKI-sensitive or resistant cells. 3-5 × 10^3 cells were seeded into 96-well plates and treated with AZD4547 (1 μM or 2.5 μM) or DMSO for 48 h after adherence. For cholesterol assay, these cells were fixed and stained with Filipin III solution (Cayman Chemical, #10009779) at a final concentration of 50 μg/mL for 30 min shielded from light and then washed with wash buffer. Images were captured and analyzed by an inverted fluorescence microscope (OLYMPUS, IX73)to determine cellular cholesterol accumulation. For neutral lipid assay, these cells were permeabilized, fixed, and stained with BODIPY 493/503 (ThermoFisher, #D3922) at a final concentration of 250 ng/mL. After staining, cells were resuspended in the buffer for flow cytometry analysis.

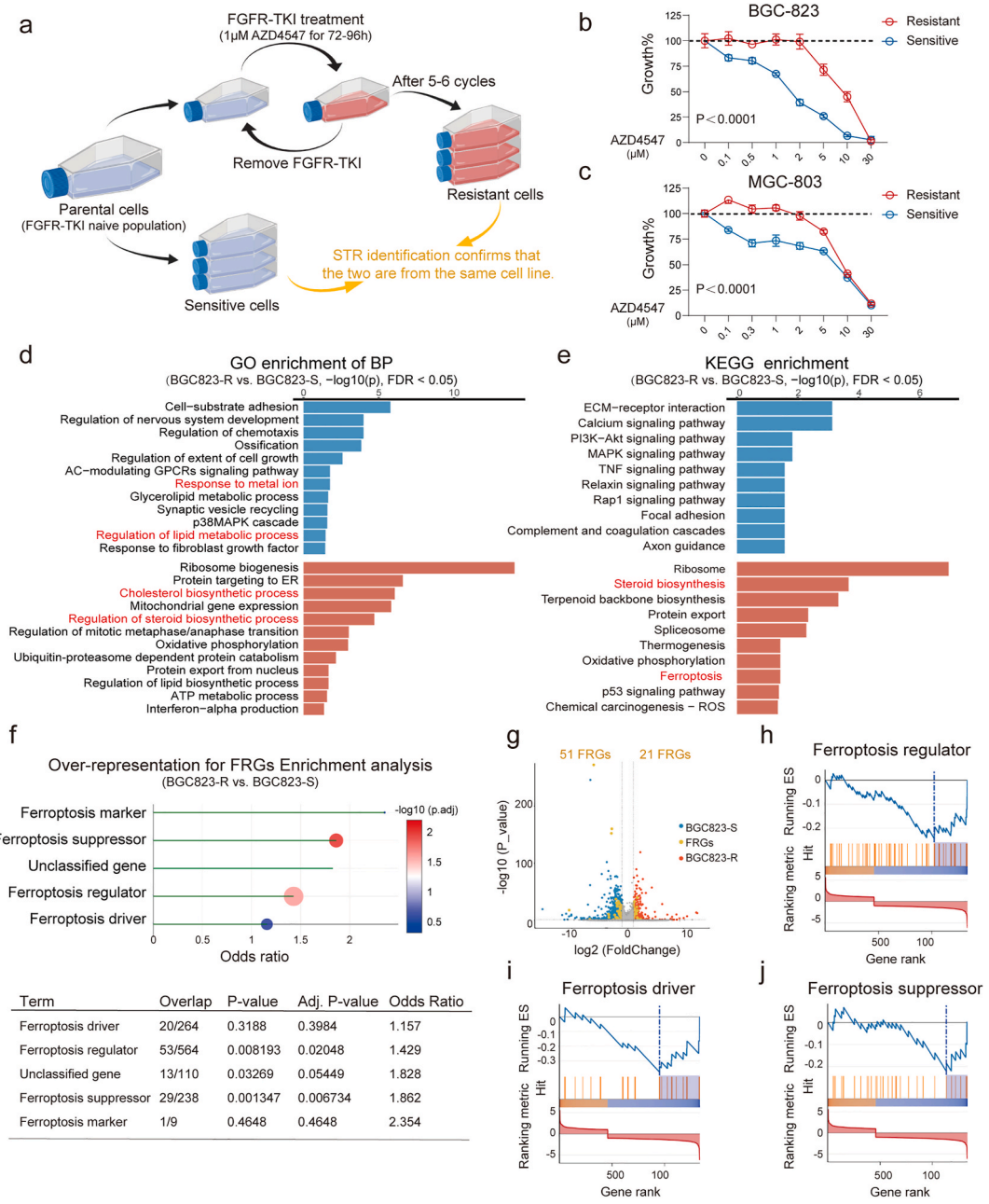

Term	Overlap	P-value	Adj. P-value	Odds Ratio
Ferroptosis driver	20/264	0.3188	0.3984	1.157
Ferroptosis regulator	53/564	0.008193	0.02048	1.429
Unclassified gene	13/110	0.03269	0.05449	1.828
Ferroptosis suppressor	29/238	0.001347	0.006734	1.862
Ferroptosis marker	1/9	0.4648	0.4648	2.354

Fig. 1. FGFR-TKI resistance is associated with ferroptosis in gastric cancer. a Scheme for the construction of FGFR-TKI-resistant GC cell lines from BGC-823 and MGC-803 through prolonged selection. **b, c** Resistant (R) and sensitive (S) cells were treated with AZD4547 (0–30 μM) for 72 h, and cell viability was measured by CCK-8 assay (n = 3 independent experiments). Statistical significance was determined by two-way ANOVA. **d, e** KEGG and GO pathway enrichment analysis of DEGs associated with FGFR-TKI resistance. **f** Over-representation for ferroptosis-related gene set enrichment analysis among DEGs using the FerrDb database. **g** Volcano plot depicting DEGs in BGC823-R vs. BGC823-S, with up-regulated genes in sensitive cells (blue), resistant cells (red), and those linked to ferroptosis (yellow). **h, i, j** GSEA of ferroptosis-related pathways for DEGs in BGC823-S vs. BGC823-R.

2.14. Animal studies

Six-week-old Balb/c-nude mice were obtained from the Animal Core Facility of Nanjing Medical University and Jiangsu Laboratory Animal Center. Tumor cells (5×10^6 cells in 100 μL PBS) were implanted by subcutaneous injection into the right axilla of the mice. Tumor progression was monitored every 3 days using calipers, with volumes calculated using the formula: volume(cm^3) = 0.5 × length (cm) × width (cm). Once tumors reached 100 mm^3, mice were treated as follows: AZD4547 (Selleck, #S2801) was administered via oral gavage at 12.5 mg/kg once daily; Ferrostatin-1 (Cayman Chemical, #17729) was injected intraperitoneally at 2.5 μmol/kg once daily; and Lovastatin (Selleck, #S2061) was delivered intratumorally at 0.44 mg/kg 12 h prior to AZD4547 administration. Treatment continued until tumors reached 1500 mm^3 or after a 15-day period, at which point mice were euthanized under anesthesia, and tumors were harvested. The study was

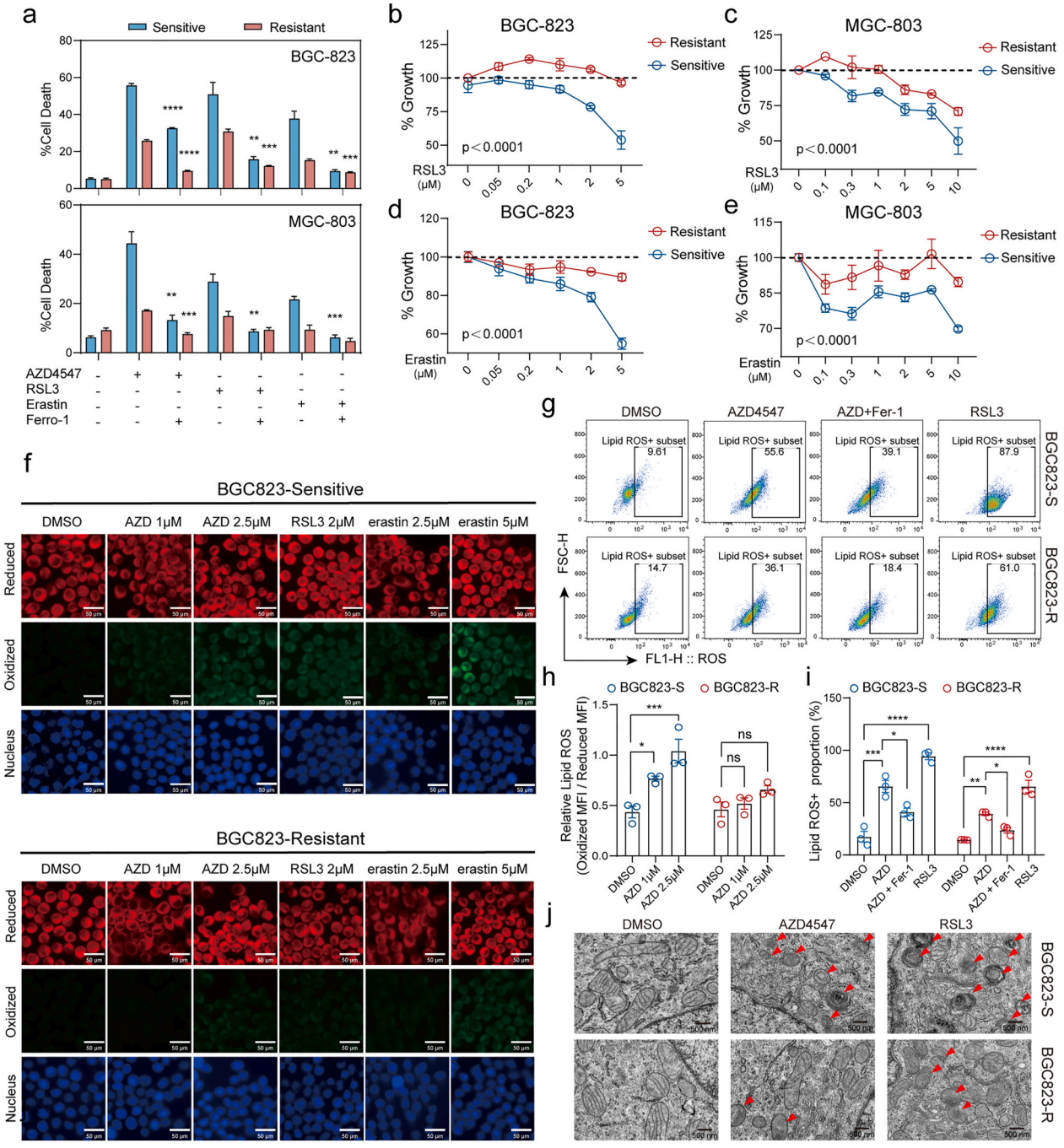

Fig. 2. Ferroptosis sensitivity is reduced in FGFR-TKI-resistant cells. a FGFR-TKI-resistant and -sensitive BGC-823 and MGC-803 cells were treated with AZD4547 (2.5 μM), RSL3 (2 μM) and erastin (5 μM) ± ferrostatin-1 (1 μM) for 48 h; cell death was assayed by PI uptake. **b-e** Cell growth in resistant and sensitive cells treated with RSL3 or Erastin for 72 h was assessed by CCK-8 assay. **f** Representative fluorescence images of oxidized lipid ROS (green), reduced lipid ROS (red) and nucleus (blue) in BGC823-S and BGC823-R treated with DMSO, AZD4547, RSL3 and erastin for 48 h (scale bars, 50 μm). **g** Flow cytometry analysis of lipid ROS + BGC823-S or BGC823-R cells treated with DMSO, AZD4547 (2.5 μM), ferrostatin-1 (1 μM) or RSL3 (2 μM) for 48 h **h, i** Quantitative analysis of lipid ROS from fluorescence microscopy (h) and FACS (i), presented as mean ± SEM. **j** Representative TEM images of BGC823-S and BGC823-R treated with DMSO, AZD4547 (2.5 μM) or RSL3 (2 μM) for 48 h showing mitochondrial alterations (red arrows). P values were determined by two-sided unpaired *t*-test (a), two-way ANOVA (b–e) and one-way ANOVA (h, i) (n = 3 independent experiments, *p < 0.05, **p < 0.01, ***p < 0.001, ****p < 0.0001).

conducted in compliance with the guidelines and regulations approved by the Institutional Animal Care and Use Committee of Nanjing Medical University (IACUC-1706007).

2.15. Statistical analysis

Statistical analyses were conducted using SPSS 22.0 and GraphPad Prism 8.0. Quantitative data were evaluated with two-sided Student's t-test or one-way ANOVA test and presented as means ± SEM. Qualitative variables were assessed using chi-squared tests. Spearman's correlation analysis determined correlation coefficients. Cox regression, Kaplan–Meier and log-rank tests were utilized for survival and prognostic factor analysis. P values < 0.05 were regarded as statistically significant. *$P < 0.05$; **$P < 0.01$; ***$P < 0.001$; ****$P < 0.0001$.

3. Results

3.1. FGFR-TKI resistance is associated with ferroptosis in gastric cancer

To investigate the mechanisms of acquired resistance to FGFR-TKI in GC, we constructed resistant cells from BGC823 and MGC803, initially sensitive due to high FGFR1 expression [18], through chronic exposure to AZD4547 (an FGFR-TKI) and prolonged selection (Fig. 1a–c). Subsequently, RNA sequencing was performed on BGC823-resistant (BGC823-R) and -sensitive (BGC823-S) cells. Gene Ontology (GO) and Kyoto Encyclopedia of Genes and Genomes (KEGG) enrichment analyses of differentially expressed genes (DEGs) between resistant and sensitive cells highlighted an enrichment in ferroptosis pathways (Fig. 1d–e). Further analysis of ferroptosis-related genes (FRGs) within these DEGs revealed an enrichment of genes involved in the regulation, promotion, and suppression of ferroptosis in FGFR-TKI-resistant cells (Fig. 1f–j). Additionally, FRGs were significantly enriched in resistant cells following FGFR-TKI treatment compared to the control group treated with DMSO (Figure S1a-b, S1d-e), while FGFR1 knockdown diminished this enrichment (Fig. S1c and S1f). Collectively, these findings suggest a potential link between acquired resistance to FGFR-TKIs in GC and ferroptosis.

3.2. Ferroptosis sensitivity is reduced in FGFR-TKI-resistant cells

Further investigation into the relationship between FGFR-TKI resistance and ferroptosis was conducted through in vitro experiments. Ferrostatin-1, a ferroptosis inhibitor, attenuated the cytotoxicity of FGFR-TKIs on sensitive cells (Fig. 2a). In contrast, resistant cells exhibited reduced sensitivity to ferroptosis induced by RSL3 (a GPX4 inhibitor) and erastin (a system Xc^- antagonist) [23,24], two canonical ferroptosis inducers (Fig. 2b–e). Lipid reactive oxygen species (ROS) levels assessed with BODIPY-581/591 C11 revealed that FGFR-TKI-sensitive cells were susceptible to lipid peroxidation, as confirmed by both fluorescence imaging and flow cytometry, whereas resistant cells were unresponsive to FGFR-TKIs or ferroptosis inducers (Fig. 2f–i, S2a-d). Similar results were observed with the DCFH-DA probe, which measures total ROS levels, showing that ferrostatin-1 diminished AZD4547-induced ROS production (Fig. S2e). Additionally, transmission electron microscopy (TEM) identified ultrastructural changes in mitochondria of AZD4547-treated sensitive cells, including membrane wrinkling, rupture, and increased density, whereas resistant cells exhibited less mitochondrial damage with preserved morphology (Fig. 2j–S2f). These data collectively suggest that FGFR-TKI can induce ferroptosis in FGFR-TKI-sensitive cells, whereas FGFR-TKI-resistant cells have a decreased sensitivity to ferroptosis.

3.3. Reduction of ferroptosis regulator CHAC1 expression in FGFR-TKI-resistant cells

To investigate the mechanisms underlying the reduced sensitivity to ferroptosis in FGFR-TKI resistant cells, we analyzed the top 20 DEGs between resistant and sensitive cells without AZD4547 treatment, identifying six genes (CHAC1, NUPR1, ASNS, SESN2, TRIB3, LCN2) involved in the regulation of ferroptosis (Fig. 3a). Validation revealed reduced mRNA and protein expression levels of CHAC1, a glutathione (GSH)-specific degrading enzyme, in FGFR-TKI-resistant cells (Fig. 3b–c, S3a), with a positive correlation to FGFR1 expression levels (Fig. 3c). Enhanced iron uptake and GSH degradation following AZD4547 treatment were observed in sensitive cells, contrasting with subtle changes in resistant cells, indicative of FGFR-TKI-induced ferroptosis resistance (Fig. 3d–f).

Given that FGFR-TKI can upregulate CHAC1 to promote ferroptosis in sensitive cells, we subsequently explored the prognostic relevance of CHAC1 expression. Despite heterogeneity in CHAC1 expression among GC patients (Fig. 3g), GC tissues consistently showed lower CHAC1 expression compared to adjacent non-tumor tissues (Fig. 3h–i). Moreover, CHAC1 was identified as an independent prognostic factor for GC patients (Table 1), with elevated expression predicting improved survival (Fig. 3j–S3b-c).

3.4. CHAC1 overexpression overcomes FGFR-TKI resistance and enhances FGFR-TKI-induced ferroptosis

We hypothesize that CHAC1 downregulation mediates ferroptosis resistance, which may lead to FGFR-TKI resistance. To investigate this, we transfected resistant cells with CHAC1-overexpressing plasmids and knocked down CHAC1 in sensitive cells using siRNA (Fig. 4a–b). Negligible impact on the growth rate of GC cells was observed after the modulation of CHAC1 expression (Fig. S4a). Overexpression of CHAC1, as shown by CCK8 assays, increased the susceptibility of FGFR-TKI-resistant cells to AZD4547. Subsequent phenotypic assessments, including colony formation, scratch wound healing, and Transwell invasion, consistently showed that elevated CHAC1 levels augmented the cytotoxicity of FGFR-TKI and amplified the inhibitory effects of FGFR-TKI on the proliferation, migration, and invasion of FGFR-TKI-resistant cells (Fig. 4d–f). Conversely, CHAC1 knockdown in sensitive cells resulted in the acquisition of FGFR-TKI resistance (Fig. S4b–f).

Moreover, the effect of CHAC1 overexpression on FGFR-TKI-induced ferroptosis sensitivity was explored, and we observed that overexpression of CHAC1 in resistant cells led to exacerbated GSH depletion and augmented susceptibility to FGFR-TKI-induced lipid peroxidation (Fig. 4g–h). Furthermore, supplementation with excess GSH or N-Acetylcysteine (NAC) in CHAC1-overexpressing resistant cells markedly reversed the enhanced FGFR-TKI cytotoxicity and lipid peroxidation (Fig. 4i–j, S4g-h). Collectively, these findings underscore the pivotal role of CHAC1 in modulating GC response to FGFR-TKI, potentially through CHAC1-mediated changes in ferroptosis sensitivity.

3.5. Increased cholesterol accumulation in FGFR-TKI-resistant cells and lipid disruption in GC microenvironment

Our analysis also revealed that differential gene expression between sensitive and FGFR-TKI-treated resistant cells was significantly enriched in pathways involved in cholesterol synthesis and lipid metabolism (Fig. 1d–e). Further examination of genes pivotal to cholesterol metabolism indicated upregulated cholesterol production and diminished transport in resistant cells (Fig. 5a–b). Filipin III staining revealed elevated intracellular cholesterol accumulation in resistant cells following FGFR-TKI treatment, characterized by increased size and number of cholesterol droplets (Fig. 5c–d). Additionally, analysis of genes involved in fatty acid (FA) and triglyceride (TG) metabolism indicated no change in the synthesis of these lipids in resistant cells (Fig. S5a). Nevertheless, resistant cells exhibited downregulation of the fatty acid transport proteins (FATPs) and fatty acid-binding proteins (FABPs) families, correlating with decreased levels of intracellular neutral lipids content compared to sensitive cells (Fig. 5e–f).

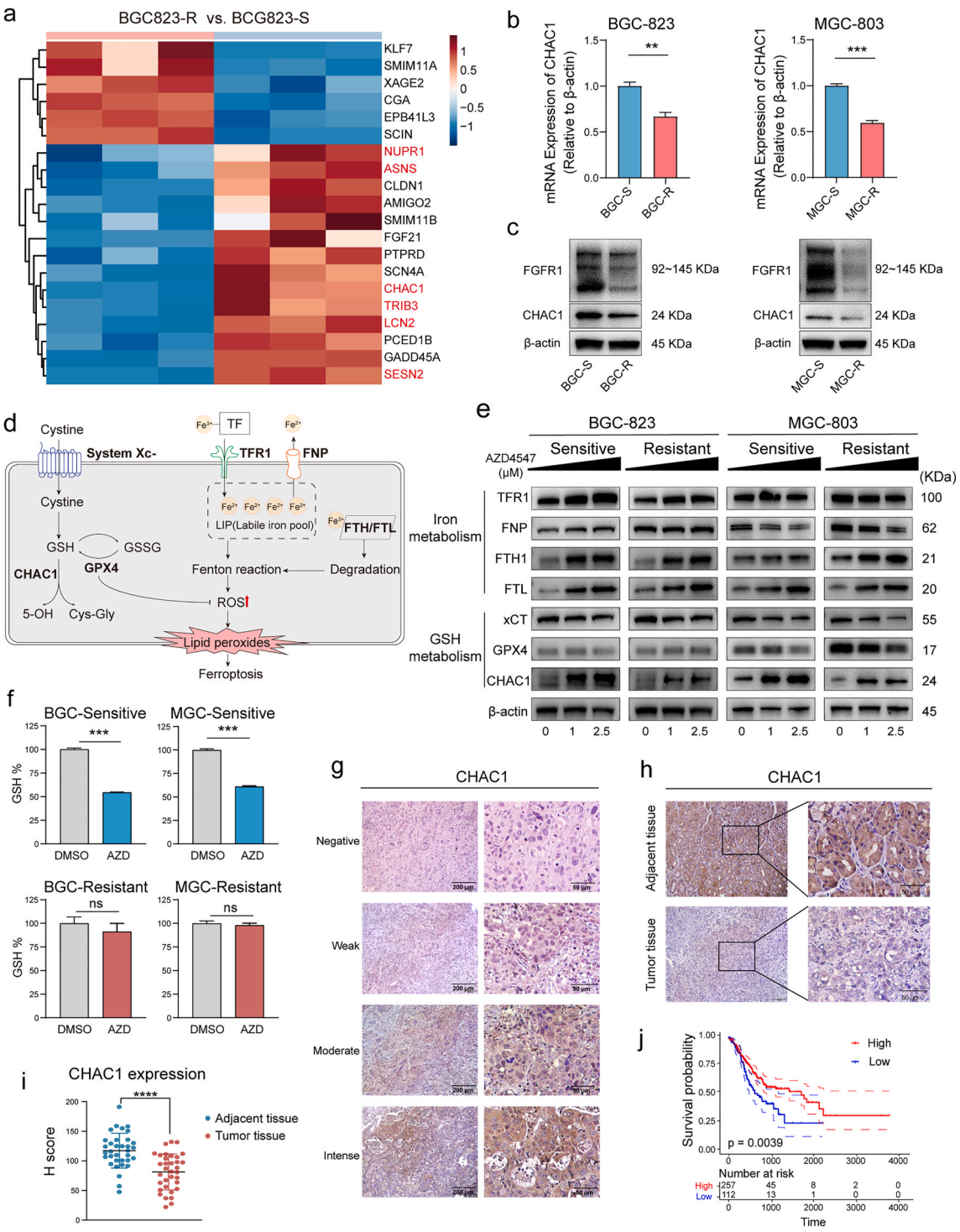

Fig. 3. Reduction of ferroptosis regulator CHAC1 expression in FGFR-TKI-resistant cells. a Heatmap depicting the top 20 DEGs from RNA-seq analysis of BGC823-R vs. BGC823-S cells, with FRGs highlighted in red. **b** qRT-PCR analysis of CHAC1 expression levels in sensitive and resistant cells. **c** Western blot assessment of FGFR1 and Chac1 protein levels in sensitive and resistant cells. **d** Schematic illustrating the role of iron and GSH metabolism-related proteins in ferroptosis development. **e** Western blot assessment of iron and GSH metabolism-related proteins in cells treated with AZD4547 for 48 h **f** GSH levels in cells treated with DMSO or 1 μM AZD4547 for 48 h **g** Representative immunohistochemistry staining images of different expression levels of CHAC1 in GC tumor tissues. **h, i** IHC staining and scoring of CHAC1 in GC tumor and adjacent normal tissues (n = 34 paired samples). **j** Kaplan–Meier curves demonstrating the correlation between CHAC1 expression levels and OS in GC patients. Data were from TCGA database. P values were calculated using two-sided unpaired *t*-test (n = 3 independent experiments, *p < 0.05, **p < 0.01, ***p < 0.001, ****p < 0.0001).

Given the reduced expression of FAs uptake-related proteins in resistant cells, we hypothesized that lipids within the tumor microenvironment (TME) may be involved in modulating the resistance of GC cells to FGFR-TKI. We characterized the lipid profiles within the GC microenvironment of 19 patients by extracting tumor interstitial fluid (TIF) from fresh surgical specimens and collecting matched serum, followed by non-targeted HPLC-MS/MS lipidomics profiling (Fig. 5g). This approach identified 15 distinct lipid classes (Fig. S5c) and detected a

Table 1
Univariate and multivariate COX regression analyses of different clinical characteristics and prognostic factors in STAD patients. (n = 369).

Variable	All case	Univariate analysis		Multivariate analysis	
		HR (95 % CI)	P value	HR (95 % CI)	P value
Gender		1.297 (0.910–1.849)	0.150		
Female	129				
Male	240				
Age (years)		1.530 (1.053–2.221)	0.026 *		
<60	118				
≥60	248				
Differentiation		1.397 (1.006–1.942)	0.046 *		
Well	9				
Moderate	126				
Poor	225				
Tumor location		1.024 (0.860–1.219)	0.790		
Gastroesophageal Junction	38				
Cardia/Proximal	50				
Fundus/Body	133				
Antrum/Distal	135				
TNM stage		1.712 (1.219–2.403)	0.002 **	1.659 (1.181–2.331)	0.004 **
I/II	171				
III/IV	196				
CHAC1 expression		0.610 (0.434–0.856)	0.004 **	0.635 (0.452–0.892)	0.009 **
Low	112				
High	257				

significant disparity in lipid composition between TIF and serum of GC (Fig. 5h-i. S5b). Specifically, in TIF, relative abundances of FA, diacylglycerols (DAG), phosphatidylethanolamine (PE), phosphatidylinositol (PI), phosphatidylserine (PS), ceramides (Cer), and sphingomyelins (SM) was significantly elevated, while phosphatidylcholine (PC), lysophosphatidylcholine (lysoPC), and phosphatidylglycerol (PG) were reduced (Fig. 5j–S5d). Overall, our findings suggest that cholesterol accumulation in FGFR-TKI-resistant cells, along with diminished fatty acid uptake via FATPs and FABPs from the lipid-disrupted GC microenvironment may be pivotal in the development of FGFR-TKI resistance.

3.6. Inhibition of exogenous FA-regulated cholesterol synthesis enhances CHAC1 and ameliorates FGFR-TKI resistance in GC

Previous studies have reported that a high-fat diet (HFD) and exogenous lipid mixtures can modulate CHAC1 expression [25]. Based on this, we explored the effects of stearic acid (SA), enriched in GC microenvironment (Fig. 5k), and other common FAs on FGFR-TKI-induced CHAC1 expression in sensitive cells expressing FATPs and FABPs. We discovered that SA combined with FGFR-TKI consistently enhanced cytotoxicity in both BGC823-S and MGC803-S cells, whereas palmitic acid (PA), oleic acid (OA), and arachidonic acid (AA) exhibited controversial effects (Fig. 6a–b). Additionally, treatment with SA was observed to amplify the FGFR-TKI-induced upregulation of CHAC1 and ROS-related genes (Fig. 6c–f). These results imply that exogenous SA uptake may potentiate FGFR-TKI-induced ferroptosis in sensitive cells.

We hypothesized that SA abundant in TIF may interact with the cholesterol synthesis pathway in FGFR-TKI-resistant cells. Our results show that exogenous SA or PA treatments reduce cholesterol accumulation (Fig. 6g). Then we explored the interplay between cholesterol synthesis and CHAC1-mediated ferroptosis sensitivity. Statin-induced inhibition of cholesterol synthesis contributed to a dose-dependent increase in CHAC1 expression (Fig. 6h), and enhanced ROS production induced by FGFR-TKI in resistant cells (Fig. 6i). Overall, our findings indicate that cholesterol accumulation in resistant cells results from diminished SA uptake, and that pharmacological inhibition of HMGCR boosts CHAC1 expression, thereby ameliorating FGFR-TKI-induced ferroptosis resistance.

3.7. Overexpression of CHAC1 or cholesterol removal enhances the anticancer activity of FGFR-TKI in vivo

To extend our in vitro findings, we conducted in vivo studies to assess the impact of CHAC1 overexpression on tumor growth. BGC823-R and MGC803-R cells with CHAC1 overexpression (CHAC1-OE) were established using a lentiviral system (Fig. S6a–b). Following subcutaneous implantation of CHAC1-OE or control vector cells into Balb/c nude mice, we observed that CHAC1 overexpression moderately inhibited the growth of FGFR-TKI-resistant tumors (Fig. 7a–c, S6c-d). Next, we explored whether overexpression of CHAC1 could enhance the sensitivity of resistant tumors to FGFR-TKI in vivo. Mice bearing CHAC1-OE or Vector tumors were administered AZD4547, either alone or combined with ferrostatin-1 (Fig. 7d). CHAC1 overexpression reversed FGFR-TKI resistance in GC; however, this effect was abrogated by ferroptosis inhibition (Fig. 7e–g, S6e-g). Finally, we assessed the impact of modulating cholesterol synthesis on FGFR-TKI efficacy and the contribution of ferroptosis. Mice harboring FGFR-TKI-resistant tumors treated with AZD4547 and lovastatin showed tumor reduction and even regression (Fig. 7h–k, S6h-j). The benefits of this combination therapy were negated by the inhibition of ferroptosis (Fig. 7i–S6h). In conclusion, our results demonstrate that overexpressing CHAC1 or inhibiting cholesterol synthesis can effectively reverse FGFR-TKI resistance in vivo, positioning CHAC1 and HMGCR as promising targets for the treatment of FGFR-TKI-resistant gastric cancer.

4. Discussion

GC remains a substantial health challenge, largely due to the scarcity of effective molecular-targeted treatments. Its molecular heterogeneity often leads to treatment failure, highlighting the need for tailored therapeutic approaches [26,27]. The FGF/FGFR signaling pathway, implicated in various cancers, is known to be aberrant in 6.7 % of GC and plays a crucial role in cancer progression [28,29]. The FGF/FGFR axis is involved in various aspects of cancer progression, including cell proliferation, survival, migration, and angiogenesis [30]. Therefore, targeting the FGF/FGFR pathway is a promising approach for GC treatment. AZD4547, a highly selective TKI for FGFR1-3, has shown antitumor efficacy in preclinical models of gastric adenocarcinoma with FGFR2 amplification [5]. However, clinical trials of FGFR inhibitors have produced inconsistent outcomes [5,31–33], suggesting a complex response pattern in GC patients. The development of drug resistance is a

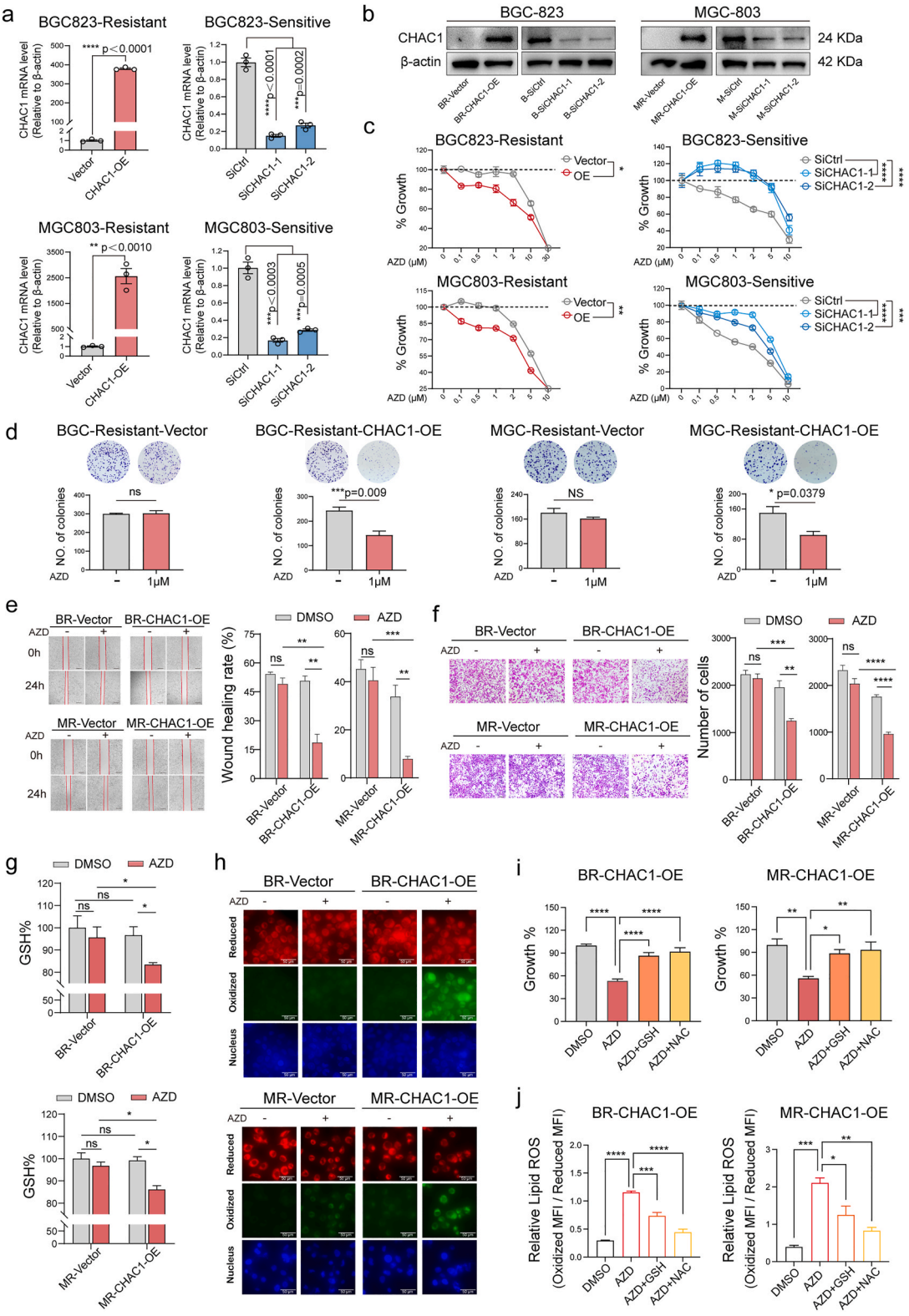

Fig. 4. CHAC1 Overexpression overcomes FGFR-TKI resistance and enhances FGFR-TKI-induced ferroptosis. a qRT-PCR analysis of CHAC1 mRNA expression in GC cells with CHAC1 overexpression or knockdown (mean ± SEM). **b** Western blot assessment of CHAC1 protein expression in GC cells with CHAC1 overexpression or knockdown. **c** CCK-8 assay evaluating AZD4547 sensitivity. **d** Crystal violet staining of AZD4547-treated cells after 3 weeks, with colony formation quantified (mean ± SEM). **e** Wound-healing assay showing cell migration at 24 h; wound closure quantified as remaining open area percentage (mean ± SEM, n = 3). **f** Transwell invasion assay with crystal violet-stained invaded cells following a 24-h 1 μM AZD4547 treatment, and quantified cell counts (mean ± SEM). **g** GSH levels in cells treated with DMSO or AZD4547 for 48 h **h** Representative fluorescence images and analysis of lipid ROS (scale bars, 50 μm). **i** BR-CHAC1-OE and MR-CHAC1-OE cells were treated with DMSO, AZD4547 (2.5 μM) with or without GSH (10 mM) and NAC (5 mM) for 72 h, and cell viability was measured by CCK-8 assay. **j** Quantitative analysis of lipid ROS from fluorescence microscopy, presented as mean ± SEM. P values were calculated using two-sided unpaired *t*-test (a, d, e, f, g), one-way ANOVA (i, j) and two-way ANOVA (c) (n = 3 independent experiments, *p < 0.05, **p < 0.01, ***p < 0.001, ****p < 0.0001).

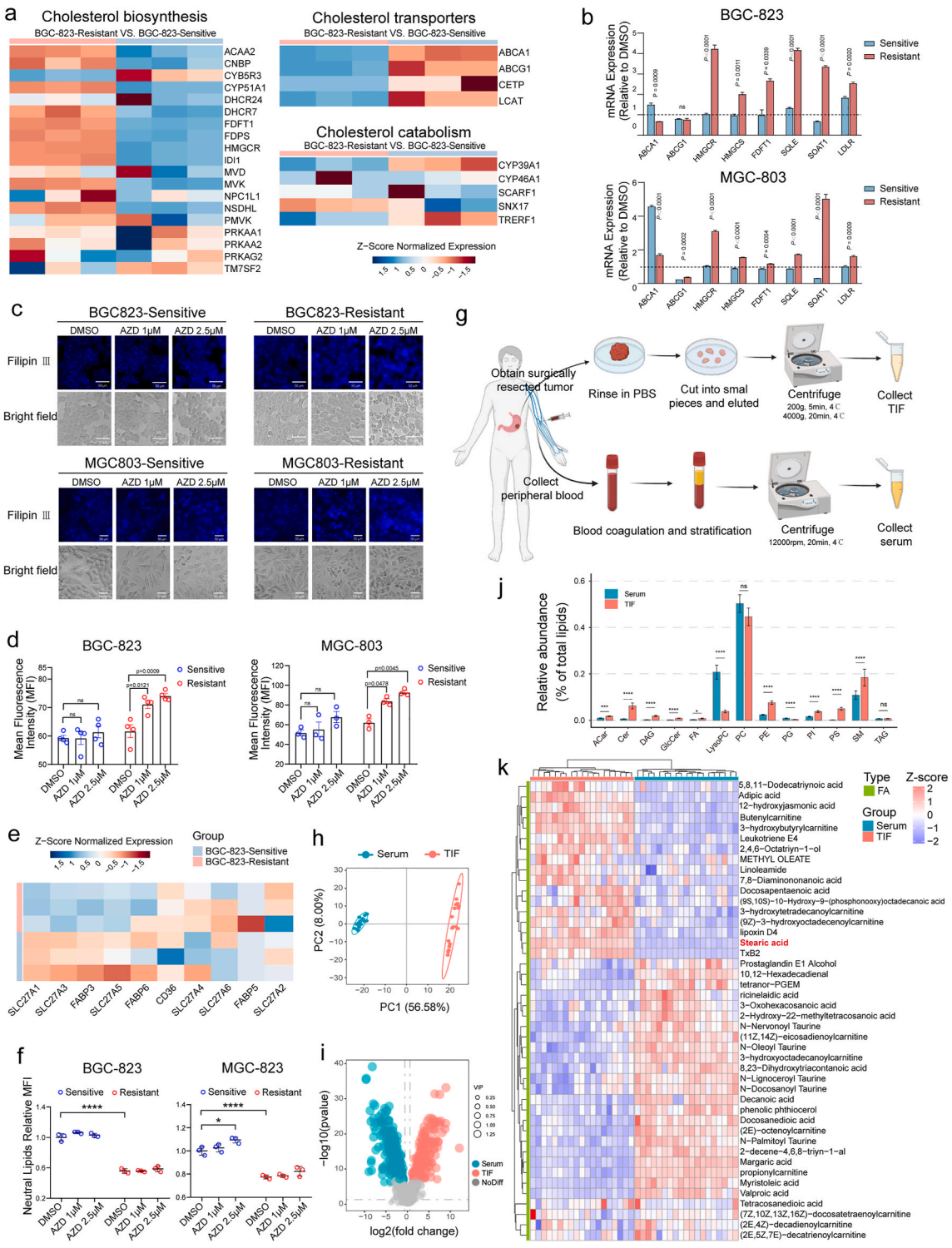

Fig. 5. Increased cholesterol accumulation in FGFR-TKI-resistant cells and lipid disruption in GC microenvironment. a Transcriptional analysis comparing BGC823-R and BGC823-S cells identified alterations of genes involved in cholesterol metabolism, displayed as log2-normalized expression levels. **b** qRT-PCR analysis of cholesterol metabolism–related enzyme gene expression (mean ± SEM). **c** Following 48-h treatment with AZD4547, gastric cells were stained with Filipin III and analyzed for cholesterol content using fluorescence microscopy (scale bars, 50 μm). **d** Mean fluorescence intensity (MFI) of Filipin III staining (mean ± SEM). **e** Transcriptional analysis of genes involved in fatty acid and triacylglycerol metabolism displayed as log2-normalized expression levels. **f** Gastric cancer cells were treated with AZD4547 and stained with BODIPY 493/503 to evaluate neutral lipid content. Flow cytometry measured the fluorescence intensity, displayed as mean ± SEM. **g** Schematic overview of the collection process for tumor interstitial fluid (TIF) and serum in GC patients, followed by lipidomic analysis using mass spectrometry (MS). **h-i** Principal component analysis (PCA) (h) and volcano plots (i) comparing lipidomic profiles between TIF and serum samples from GC patients (n = 19 paired samples). **j** Relative abundance of lipid species in TIF and serum from GC patients. **k** Heatmaps of differentially expressed fatty acids in TIF and serum from GC patients (shown as Z score). P values were calculated using two-sided unpaired *t*-test (a) and one-way ANOVA (d, f) (n = 3 independent experiments, *p < 0.05, **p < 0.01, ***p < 0.001, ****p < 0.0001).

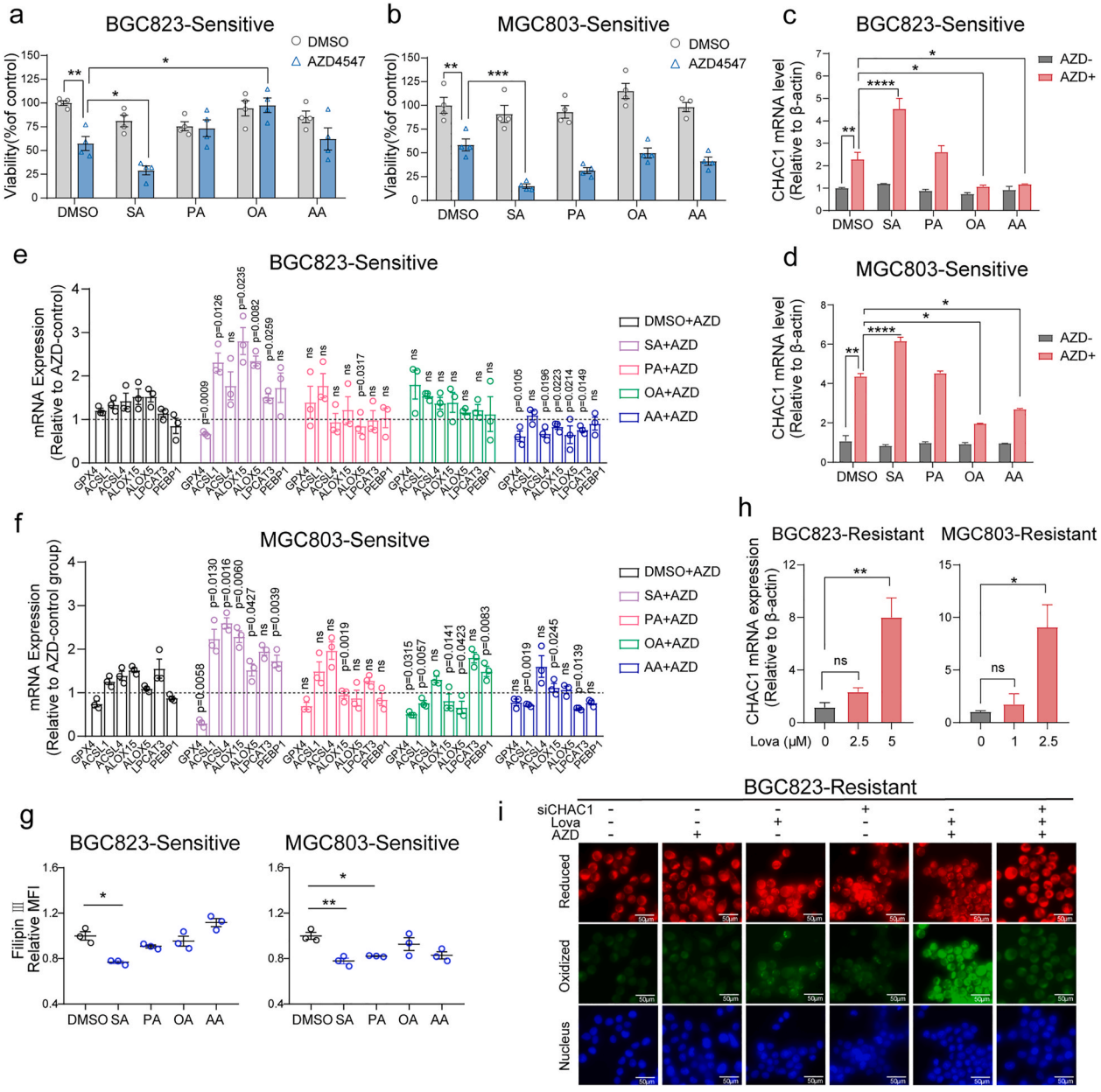

Fig. 6. Accumulated cholesterol induced by exogenous fatty acids downregulates CHAC1, contributing to FGFR-TKI resistance in GC. a, b Following 48-h incubation with AZD4547 or DMSO ± indicated lipids, cell viability in GC cells was evaluated using CCK-8 assay. **c, d, e, f** qRT-PCR analysis of CHAC1 and ROS-related genes in GC cells with AZD4547 or DMSO ± indicated lipids (mean ± SEM). **g** Sensitive cells were treated with indicated lipids and stained with Filipin III to evaluate cholesterol content. MFI was measured using flow cytometry (mean ± SEM). **h** Lovastatin-treated resistant cells were assessed for CHAC1 mRNA expression using qRT-PCR. **i** Representative fluorescence images and analysis of lipid ROS (scale bars, 50 μm). P values were calculated using two-way ANOVA (a, b, c, d, e, f) and one-way ANOVA (g, h) (n = 3 independent experiments, *p < 0.05, **p < 0.01, ***p < 0.001, ****p < 0.0001).

likely contributor to the variable efficacy of FGFR-TKI, warranting further exploration. Accordingly, our study uncovers a potential evasion mechanism in GC cells against the cytotoxic effects of FGFR-TKI, highlighting the interplay between ferroptosis and lipid metabolism in resistance development (Fig. 7j).

The role of ferroptosis in anticancer therapies resistance is gaining recognition. This iron-dependent form of cell death can be triggered by molecular targeted drugs like sorafenib and lapatinib [34,35]. Studies have shown that drug-resistant tumor cells stabilize Nrf2 via Keap1 inactivation or Nrf2 pathway mutations, controlling GSH biosynthesis and antioxidant responses, and thereby promoting resistance to ferroptosis and other cancer therapies [36]. However, the relationship between FGFR-TKI resistance and ferroptosis has not been reported previously. Our research indicates that FGFR-TKI can induce ferroptosis in GC cells, but resistance to this process is a hallmark of FGFR-TKI-resistant cells.

Inefficient lipid peroxidation repair protects cancer cells from ferroptosis [37]. We identified glutathione-specific γ-glutamylcyclotransferase 1 (CHAC1) as a key player in FGFR-TKI resistance, which specifically degrades antioxidant GSH to 5-oxoproline and Cys-Gly dipeptide, thereby sustaining intracellular oxidative homeostasis [38,39]. Although CHAC1 has been identified as a key gene regulating ferroptosis in the processes of ischemic stroke and colitis-associated carcinogenesis [25,40], its impact on FGFR-TKI resistance still needs further investigation. We link CHAC1 downregulation to ferroptosis resistance and imply that its overexpression could enhance the cytotoxic effects of FGFR-TKI by regulating the lipid peroxidation repair system. In addition, our results suggest that CHAC1 expression is related to

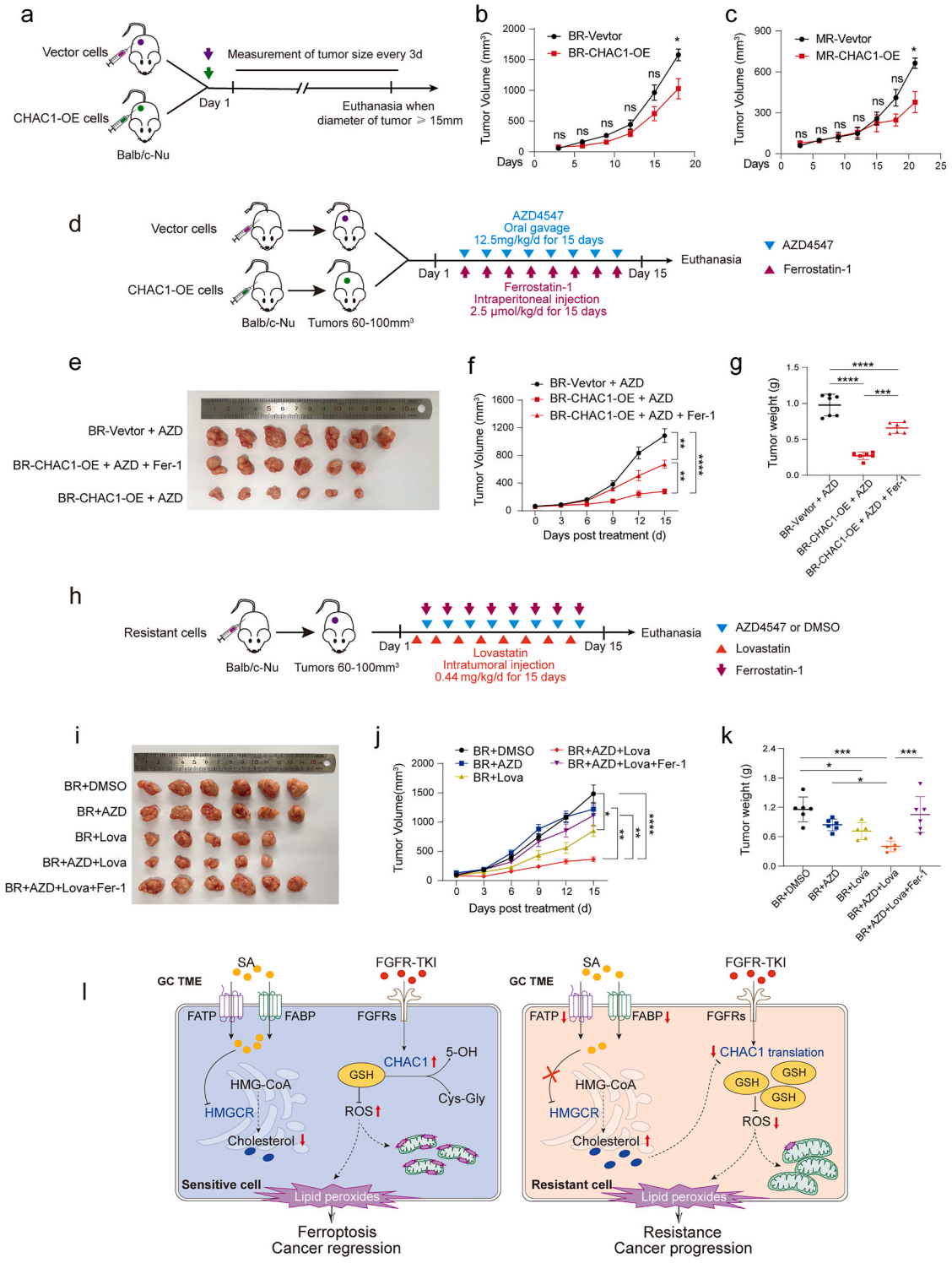

Fig. 7. Overexpression of CHAC1 or cholesterol removal enhances the anticancer activity of FGFR-TKI in vivo. **a** Diagram of the subcutaneous tumor implantation procedure in Balb/c nude mice, with a timeline for monitoring tumor growth and dimensions. **b-c** Tumor growth curves depict tumor volume measurements in mice harboring BGC823-Vector or BGC823-CHAC1-OE tumors (b, n = 6 mice per group), and MGC803-Vector or MGC803-CHAC1-OE tumors (c, n = 4 mice per group), presented as mean ± SEM. **d** Schematic of Balb/c nude mice harboring BR-Vector or BR-CHAC1-OE subcutaneous tumors treated at indicated times with AZD4547 ± ferrostatin-1. **e-g** Representative photograph (e), tumor growth curves (f) and weights (g) of subcutaneous BR-Vector or BR-CHAC1-OE tumors in Balb/c nude mice treated with AZD4547 ± ferrostatin-1 (BR-Vevtor + AZD, n = 7 mice; BR-CHAC1-OE + AZD + Fer-1, BR-CHAC1-OE + AZD, n = 6 mice). **h** Schematic of Balb/c nude mice harboring BGC823-R tumors treated at indicated times with DMSO, AZD4547, lovastatin ± ferrostatin-1. **i-k** Representative photograph (i), tumor growth curves (j) and weights (k) of subcutaneous BR tumors in Balb/c nude mice treated with DMSO, AZD4547, lovastatin ± ferrostatin-1 (BR + DMSO, BR + AZD, BR + AZD + Lova + Fer-1, n = 6 mice; BR + Lova, BR + AZD + Lova, n = 5 mice). P values were calculated using two-way ANOVA (b, c, f, j) and one-way ANOVA (g, k) (*p < 0.05, **p < 0.01, ***p < 0.001, ****p < 0.0001).

FGFR1 expression and immune scores (Fig. 3c–S3d), which may also contribute to the mechanism of CHAC1 downregulation-induced FGFR-TKI resistance. Our study underscores the importance of CHAC1-mediated ferroptosis in FGFR-TKI resistance and suggests that CHAC1 may predict responses to FGFR-TKI.

Dysregulated lipid homeostasis has been firmly closely tied to tumor progression and therapeutic resistance in gastric and other cancers, influencing cell growth and survival, and driving drug resistance via metabolic reprogramming and alterations in TME [41–43]. Studies show that resistant cells typically exhibit increased lipid droplets (LDs) containing triglycerides and cholesterol esters, enhanced contact between LDs and mitochondria, and elevated lipid synthesis [44]. Additionally, disruption of cholesterol homeostasis induces metabolic reprogramming in breast cancer (BC) cells, leading to enhanced resistance to ferroptosis and consequently driving a significant increase in the tumorigenicity and metastatic potential of BC [45]. Similarly, our research reveals that FGFR-TKI-resistant GC cells exhibit significant reprogramming of lipid metabolism, notably cholesterol accumulation and reduced fatty acid uptake. Moreover, targeting cholesterol synthesis appears to effectively reverse FGFR-TKI resistance, highlighting the pivotal role of lipid metabolism in therapeutic outcomes.

The connection between lipid metabolism and ferroptosis represents another significant frontier in current cancer research. Research has shown that diverse lipid species, including fatty acyls, glycerolipids, glycerophospholipids, and sterol lipids, significantly influence cellular susceptibility to ferroptosis [46]. For instance, exogenous cholesterol and OA uptake may diminish RSL3-induced ferroptosis, whereas PA can potentiate this response [25]. Recent studies have reported that 7-Dehydrocholesterol (7-DHC) can act as an endogenous inhibitor of ferroptosis, regulating its sensitivity [47,48]. However, the role of the various lipids abundant in the TME in FGFR-TKI-induced ferroptosis sensitivity remains unclear in GC. Our study highlights the significance of lipid profiling in deciphering the contribution of the TME to FGFR-TKI resistance in GC. We found SA enrichment in TIF enhances cholesterol synthesis and promotes ferroptosis induced by FGFR-TKI. Additionally, FGFR-TKI-resistant cells adapt to the metabolic stress induced by FGFR-TKI by downregulating FATPs and FABPs, which leads to decreased SA uptake and cholesterol accumulation, and impairs the peroxidation repair system and FGFR-TKI sensitivity. The identification of TIF lipid profile and their correlation with FGFR-TKI resistance provides new insights for potentiating the effectiveness of FGFR-TKI.

Our findings hold crucial clinical implications for the development of novel therapeutic strategies targeting GC patients with FGFR-TKI resistance. By elucidating the roles of ferroptosis and lipid metabolism in FGFR-TKI resistance, we can offer more personalized strategies for patients with FGF/FGFR functional alterations. Our in vivo study results indicate that targeting CHAC1 overexpression or cholesterol synthesis can effectively reverse FGFR-TKI resistance and enhance its anticancer activity, with these approaches being contingent on ferroptosis, potentially offering new therapeutic avenues to overcome drug resistance. Furthermore, our research highlights the analysis of lipid profiling in TME, which may aid in identifying new biomarkers to improve patient prognosis and treatment response.

While our study offers new insights into the association between FGFR-TKI resistance, ferroptosis, and lipid metabolism, there are limitations to consider. Our research primarily focuses on in vitro cell culture models and animal models, which may not fully replicate the complexities of the human body. Future studies should validate our findings in larger patient cohorts and explore additional biomarkers that could influence FGFR-TKI resistance. Moreover, although we have identified the roles of CHAC1 and cholesterol synthesis in FGFR-TKI-induced ferroptosis, the precise molecular mechanisms warrant further investigation.

In summary, our research uncovers the complexity of FGFR-TKI resistance in GC and lays the groundwork for exploring novel therapies. Translating these findings into clinical practice will require further research and validation but holds the potential to improve patient outcomes in GC.

CRediT authorship contribution statement

Jingwen Chen: Writing – original draft, Visualization, Methodology, Investigation, Data curation, Conceptualization. **Yedi Huang:** Writing – original draft, Validation, Methodology, Investigation, Data curation, Conceptualization. **Daocheng Zuo:** Methodology, Investigation. **Ruimin Shan:** Validation, Data curation. **Songmao Li:** Methodology, Investigation. **Ran Li:** Methodology. **Dong Hua:** Visualization, Writing – original draft. **Qiang Zhan:** Writing – review & editing, Conceptualization. **Xudong Song:** Data curation, Validation. **Yun Chen:** Methodology, Funding acquisition, Conceptualization. **Pei Ma:** Writing – review & editing, Investigation, Funding acquisition. **Ling Ma:** Resources, Funding acquisition, Conceptualization. **Guoquan Tao:** Conceptualization, Funding acquisition, Resources, Writing – review & editing. **Yongqian Shu:** Writing – review & editing, Resources, Funding acquisition, Conceptualization.

Data availability statement

The data sets supporting the findings of this study are available upon reasonable request from the corresponding author.

Funding statement

This work was supported by National Natural Science Foundation of China (82102981,82172889, 82173347), Jiangsu Provincial Key Research Development Program of China (BE2022770), Jiangsu Provincial Medical Innovation Center (CXZX202204), Jiangsu Provincial Medical Key Discipline Cultivation Unit (JSDW202233), Jiangsu Province Hospital High-level Talent Cultivation Program (Phase I) (CZ0121002010037), Postdoctoral Science Foundation of China (no. 2024M751224), Nanjing Postdoctoral Research Funding Program and Qing Lan Project of JiangSu Province, Postgraduate Research & Practice Innovation Program of Jiangsu Province (KYCX24_2037), Beijing Xisike Clinical Oncology Research Foundation (Y-2022METAZQN-0012).

Declaration of competing interest

The authors declare that they have no known competing financial interests or personal relationships that could have appeared to influence the work reported in this paper.

Appendix A. Supplementary data

Supplementary data to this article can be found online at https://doi.org/10.1016/j.redox.2025.103693.

Data availability

Data will be made available on request.

References

[1] A.P. Thrift, T.N. Wenker, H.B. El-Serag, Global burden of gastric cancer: epidemiological trends, risk factors, screening and prevention, Nat. Rev. Clin. Oncol. 20 (2023) 338–349.

[2] F.H. Wang, X.T. Zhang, L. Tang, Q. Wu, M.Y. Cai, Y.F. Li, X.J. Qu, H. Qiu, Y. J. Zhang, J.E. Ying, J. Zhang, L.Y. Sun, R.B. Lin, C. Wang, H. Liu, M.Z. Qiu, W. L. Guan, S.X. Rao, J.F. Ji, Y. Xin, W.Q. Sheng, H.M. Xu, Z.W. Zhou, A.P. Zhou, J. Jin, X.L. Yuan, F. Bi, T.S. Liu, H. Liang, Y.Q. Zhang, G.X. Li, J. Liang, B.R. Liu, L. Shen, J. Li, R.H. Xu, The Chinese Society of Clinical Oncology (CSCO): clinical guidelines for the diagnosis and treatment of gastric cancer, 2023, Cancer Commun. 44 (2024) 127–172.

[3] R.J. Huang, M. Laszkowska, H. In, J.H. Hwang, M. Epplein, Controlling gastric cancer in a World of heterogeneous risk, Gastroenterology (New York, N. Y., 1943) 164 (2023) 736–751.

[4] L. Xie, X. Su, L. Zhang, X. Yin, L. Tang, X. Zhang, Y. Xu, Z. Gao, K. Liu, M. Zhou, B. Gao, D. Shen, L. Zhang, J. Ji, P.R. Gavine, J. Zhang, E. Kilgour, X. Zhang, Q. Ji, FGFR2 gene amplification in gastric cancer predicts sensitivity to the selective FGFR inhibitor AZD4547, Clin. Cancer Res. : an official journal of the American Association for Cancer Research 19 (2013) 2572–2583.
[5] C. Hierro, M. Alsina, M. Sánchez, V. Serra, J. Rodon, J. Tabernero, Targeting the fibroblast growth factor receptor 2 in gastric cancer: promise or pitfall? Ann. Oncol. : official journal of the European Society for Medical Oncology 28 (2017) 1207–1216.
[6] V. Pozzi, R. Campagna, D. Sartini, M. Emanuelli, Nicotinamide N-Methyltransferase as promising tool for management of gastrointestinal Neoplasms, Biomolecules 12 (2022) 1173.
[7] G. Lei, L. Zhuang, B. Gan, The roles of ferroptosis in cancer: tumor suppression, tumor microenvironment, and therapeutic interventions, Cancer Cell 42 (2024) 513–534.
[8] J. Le, G. Pan, C. Zhang, Y. Chen, A.K. Tiwari, J.J. Qin, Targeting ferroptosis in gastric cancer: strategies and opportunities, Immunol. Rev. 321 (2024) 228–245.
[9] X. Tong, R. Tang, M. Xiao, J. Xu, W. Wang, B. Zhang, J. Liu, X. Yu, S. Shi, Targeting cell death pathways for cancer therapy: recent developments in necroptosis, pyroptosis, ferroptosis, and cuproptosis research, J. Hematol. Oncol. 15 (2022) 174.
[10] C. Zhang, X. Liu, S. Jin, Y. Chen, R. Guo, Ferroptosis in cancer therapy: a novel approach to reversing drug resistance, Mol. Cancer 21 (2022) 47.
[11] X. Mao, J. Xu, M. Xiao, C. Liang, J. Hua, J. Liu, W. Wang, X. Yu, Q. Meng, S. Shi, ARID3A enhances chemoresistance of pancreatic cancer via inhibiting PTEN-induced ferroptosis, Redox Biol. 73 (2024) 103200.
[12] A.R. Terry, N. Hay, Emerging targets in lipid metabolism for cancer therapy, Trends Pharmacol. Sci. (2024).
[13] M. Xiao, J. Xu, W. Wang, B. Zhang, J. Liu, J. Li, H. Xu, Y. Zhao, X. Yu, S. Shi, Functional significance of cholesterol metabolism in cancer: from threat to treatment, Exp. Mol. Med. 55 (2023) 1982–1995.
[14] D.H. Kim, N.Y. Song, H. Yim, Targeting dysregulated lipid metabolism in the tumor microenvironment, Arch Pharm. Res. (Seoul) 46 (2023) 855–881.
[15] G. Luis, A. Godfroid, S. Nishiumi, J. Cimino, S. Blacher, E. Maquoi, C. Wery, A. Collignon, R. Longuespée, L. Montero-Ruiz, I. Dassoul, N. Maloujahmoum, C. Pottier, G. Mazzucchelli, E. Depauw, A. Bellahcène, M. Yoshida, A. Noel, N. E. Sounni, Tumor resistance to ferroptosis driven by Stearoyl-CoA Desaturase-1 (SCD1) in cancer cells and Fatty Acid Biding Protein-4 (FABP4) in tumor microenvironment promote tumor recurrence, Redox Biol. 43 (2021) 102006.
[16] P. Liao, W. Wang, W. Wang, I. Kryczek, X. Li, Y. Bian, A. Sell, S. Wei, S. Grove, J. K. Johnson, P.D. Kennedy, M. Gijón, Y.M. Shah, W. Zou, CD8(+) T cells and fatty acids orchestrate tumor ferroptosis and immunity via ACSL4, Cancer Cell 40 (2022) 365–378.e366.
[17] J.Y. Lee, M. Nam, H.Y. Son, K. Hyun, S.Y. Jang, J.W. Kim, M.W. Kim, Y. Jung, E. Jang, S.J. Yoon, J. Kim, J. Kim, J. Seo, J.K. Min, K.J. Oh, B.S. Han, W.K. Kim, K. H. Bae, J. Song, J. Kim, Y.M. Huh, G.S. Hwang, E.W. Lee, S.C. Lee, Polyunsaturated fatty acid biosynthesis pathway determines ferroptosis sensitivity in gastric cancer, Proc. Natl. Acad. Sci. U. S. A 117 (2020) 32433–32442.
[18] R. Peng, Y. Chen, L. Wei, G. Li, D. Feng, S. Liu, R. Jiang, S. Zheng, Y. Chen, Resistance to FGFR1-targeted therapy leads to autophagy via TAK1/AMPK activation in gastric cancer, Gastric Cancer : official journal of the International Gastric Cancer Association and the Japanese Gastric Cancer Association 23 (2020) 988–1002.
[19] L. Zhao, Y. Peng, S. He, R. Li, Z. Wang, J. Huang, X. Lei, G. Li, Q. Ma, Apatinib induced ferroptosis by lipid peroxidation in gastric cancer, Gastric Cancer : official journal of the International Gastric Cancer Association and the Japanese Gastric Cancer Association 24 (2021) 642–654.
[20] S. Xu, O. Chaudhary, P. Rodríguez-Morales, X. Sun, D. Chen, R. Zappasodi, Z. Xu, A.F.M. Pinto, A. Williams, I. Schulze, Y. Farsakoglu, S.K. Varanasi, J.S. Low, W. Tang, H. Wang, B. McDonald, V. Tripple, M. Downes, R.M. Evans, N. A. Abumrad, T. Merghoub, J.D. Wolchok, M.N. Shokhirev, P.C. Ho, J.L. Witztum, B. Emu, G. Cui, S.M. Kaech, Uptake of oxidized lipids by the scavenger receptor CD36 promotes lipid peroxidation and dysfunction in CD8(+) T cells in tumors, Immunity (Camb., Mass.) 54 (2021) 1561–1577.e1567.
[21] C. Matas-Nadal, J.J. Bech-Serra, M. Guasch-Vallés, J.M. Fernández-Armenteros, C. Barceló, J.M. Casanova, C. de la Torre Gómez, R. Aguayo Ortiz, E. Garí, Evaluation of tumor interstitial fluid-extraction methods for proteome analysis: comparison of biopsy elution versus centrifugation, J. Proteome Res. 19 (2020) 2598–2605.
[22] A.C. Guyton, H.J. Granger, A.E. Taylor, Interstitial fluid pressure, Physiol. Rev. 51 (1971) 527–563.
[23] W.S. Yang, R. SriRamaratnam, M.E. Welsch, K. Shimada, R. Skouta, V. S. Viswanathan, J.H. Cheah, P.A. Clemons, A.F. Shamji, C.B. Clish, et al., Regulation of ferroptotic cancer cell death by GPX4, Cell 156 (2014) 317–331, 2014.
[24] S.J. Dixon, K.M. Lemberg, M.R. Lamprecht, R. Skouta, E.M. Zaitsev, C.E. Gleason, D.N. Patel, A.J. Bauer, A.M. Cantley, W.S. Yang, et al., Ferroptosis: an iron-dependent form of nonapoptotic cell death, Cell 149 (2012) 1060–1072.
[25] X. Zhang, W. Li, Y. Ma, X. Zhao, L. He, P. Sun, H. Wang, High-fat diet aggravates colitis-associated carcinogenesis by evading ferroptosis in the ER stress-mediated pathway, Free Radic. Biol. Med. 177 (2021) 156–166.
[26] Y. Nakamura, A. Kawazoe, F. Lordick, Y.Y. Janjigian, K. Shitara, Biomarker-targeted therapies for advanced-stage gastric and gastro-oesophageal junction cancers: an emerging paradigm, Nat. Rev. Clin. Oncol. 18 (2021) 473–487.
[27] M. Alsina, V. Arrazubi, M. Diez, J. Tabernero, Current developments in gastric cancer: from molecular profiling to treatment strategy, Nature reviews, Gastroenterol. Hepatol. 20 (2023) 155–170.
[28] Z.N. Lei, Q.X. Teng, Q. Tian, W. Chen, Y. Xie, K. Wu, Q. Zeng, L. Zeng, Y. Pan, Z. S. Chen, Y. He, Signaling pathways and therapeutic interventions in gastric cancer, Signal Transduct. Targeted Ther. 7 (2022) 358.
[29] T. Helsten, S. Elkin, E. Arthur, B.N. Tomson, J. Carter, R. Kurzrock, The FGFR landscape in cancer: analysis of 4,853 tumors by next-generation sequencing, Clin. Cancer Res. : an official journal of the American Association for Cancer Research 22 (2016) 259–267.
[30] M. Katoh, Y. Loriot, G. Brandi, S. Tavolari, Z.A. Wainberg, M. Katoh, FGFR-targeted therapeutics: clinical activity, mechanisms of resistance and new directions, Nat. Rev. Clin. Oncol. 21 (2024) 312–329.
[31] E. Van Cutsem, Y.J. Bang, W. Mansoor, R.D. Petty, Y. Chao, D. Cunningham, D. R. Ferry, N.R. Smith, P. Frewer, J. Ratnayake, P.K. Stockman, E. Kilgour, D. Landers, A randomized, open-label study of the efficacy and safety of AZD4547 monotherapy versus paclitaxel for the treatment of advanced gastric adenocarcinoma with FGFR2 polysomy or gene amplification, Ann. Oncol. : official journal of the European Society for Medical Oncology 28 (2017) 1316–1324.
[32] Z.A. Wainberg, P.C. Enzinger, Y.K. Kang, S. Qin, K. Yamaguchi, I.H. Kim, A. Saeed, S.C. Oh, J. Li, H.M. Turk, A. Teixeira, C. Borg, E. Hitre, A.A. Udrea, G.G. Cardellino, R.G. Sanchez, H. Collins, S. Mitra, Y. Yang, D.V.T. Catenacci, K.W. Lee, Bemarituzumab in patients with FGFR2b-selected gastric or gastro-oesophageal junction adenocarcinoma (FIGHT): a randomised, double-blind, placebo-controlled, phase 2 study, Lancet Oncol. 23 (2022) 1430–1440.
[33] F. Meric-Bernstam, R. Bahleda, C. Hierro, M. Sanson, J. Bridgewater, H.T. Arkenau, B. Tran, R.K. Kelley, J.O. Park, M. Javle, Y. He, K.A. Benhadji, L. Goyal, Futibatinib, an irreversible FGFR1-4 inhibitor, in patients with advanced solid tumors harboring FGF/FGFR aberrations: a phase I dose-expansion study, Cancer Discov. 12 (2022) 402–415.
[34] S.H. Hao, X.D. Ma, L. Xu, J.D. Xie, Z.H. Feng, J.W. Chen, R.X. Chen, F.W. Wang, Y. H. Tang, D. Xie, M.Y. Cai, Dual specific phosphatase 4 suppresses ferroptosis and enhances sorafenib resistance in hepatocellular carcinoma, Drug Resist. Updates : reviews and commentaries in antimicrobial and anticancer chemotherapy 73 (2024) 101052.
[35] S. Ma, E.S. Henson, Y. Chen, S.B. Gibson, Ferroptosis is induced following siramesine and lapatinib treatment of breast cancer cells, Cell Death Dis. 7 (2016) e2307.
[36] J. Lee, J.L. Roh, Targeting Nrf2 for ferroptosis-based therapy: implications for overcoming ferroptosis evasion and therapy resistance in cancer, Biochim. Biophys. Acta, Mol. Basis Dis. 1869 (2023) 166788.
[37] X. Jiang, B.R. Stockwell, M. Conrad, Ferroptosis: mechanisms, biology and role in disease, Nat. Rev. Mol. Cell Biol. 22 (2021) 266–282.
[38] A. Kumar, S. Tikoo, S. Maity, S. Sengupta, S. Sengupta, A. Kaur, A.K. Bachhawat, Mammalian proapoptotic factor ChaC1 and its homologues function as γ-glutamyl cyclotransferases acting specifically on glutathione, EMBO Rep. 13 (2012) 1095–1101.
[39] B. Niu, K. Liao, Y. Zhou, T. Wen, G. Quan, X. Pan, C. Wu, Application of glutathione depletion in cancer therapy: enhanced ROS-based therapy, ferroptosis, and chemotherapy, Biomaterials 277 (2021) 121110.
[40] Y. Wang, H. Niu, L. Li, J. Han, Z. Liu, M. Chu, X. Sha, J. Zhao, Anti-CHAC1 exosomes for nose-to-brain delivery of miR-760-3p in cerebral ischemia/reperfusion injury mice inhibiting neuron ferroptosis, J. Nanobiotechnol. 21 (2023) 109.
[41] Y. Yang, X. Liu, D. Yang, L. Li, S. Li, S. Lu, N. Li, Interplay of CD36, autophagy, and lipid metabolism: insights into cancer progression, Metab., Clin. Exp. 155 (2024) 155905.
[42] R. Vishwa, B. BharathwajChetty, S. Girisa, B.S. Aswani, M.S. Alqahtani, M. Abbas, M. Hegde, A.B. Kunnumakkara, Lipid metabolism and its implications in tumor cell plasticity and drug resistance: what we learned thus far? Cancer Metastasis Rev. 43 (2024) 293–319.
[43] Q. Xiao, M. Xia, W. Tang, H. Zhao, Y. Chen, J. Zhong, The lipid metabolism remodeling: a hurdle in breast cancer therapy, Cancer Lett. 582 (2024) 216512.
[44] A.J. Hoy, S.R. Nagarajan, L.M. Butler, Tumour fatty acid metabolism in the context of therapy resistance and obesity, Nat. Rev. Cancer 21 (2021) 753–766.
[45] W. Liu, B. Chakraborty, R. Safi, D. Kazmin, C.Y. Chang, D.P. McDonnell, Dysregulated cholesterol homeostasis results in resistance to ferroptosis increasing tumorigenicity and metastasis in cancer, Nat. Commun. 12 (2021) 5103.
[46] D. Li, Y. Li, The interaction between ferroptosis and lipid metabolism in cancer, Signal Transduct. Targeted Ther. 5 (2020) 108.
[47] Y. Li, Q. Ran, Q. Duan, J. Jin, Y. Wang, L. Yu, C. Wang, Z. Zhu, X. Chen, L. Weng, Z. Li, J. Wang, Q. Wu, H. Wang, H. Tian, S. Song, Z. Shan, Q. Zhai, H. Qin, S. Chen, L. Fang, H. Yin, H. Zhou, X. Jiang, P. Wang, 7-Dehydrocholesterol dictates ferroptosis sensitivity, Nature 626 (2024) 411–418.
[48] F.P. Freitas, H. Alborzinia, A.F. Dos Santos, P. Nepachalovich, L. Pedrera, O. Zilka, A. Inague, C. Klein, N. Aroua, K. Kaushal, B. Kast, S.M. Lorenz, V. Kunz, H. Nehring, T.N. Xavier da Silva, Z. Chen, S. Atici, S.G. Doll, E.L. Schaefer, I. Ekpo, W. Schmitz, A. Horling, P. Imming, S. Miyamoto, A.M. Wehman, T.C. Genaro-Mattos, K. Mirnics, L. Kumar, J. Klein-Seetharaman, S. Meierjohann, I. Weigand, M. Kroiss, G.W. Bornkamm, F. Gomes, L.E.S. Netto, M.B. Sathian, D.B. Konrad, D. F. Covey, B. Michalke, K. Bommert, R.C. Bargou, A. Garcia-Saez, D.A. Pratt, M. Fedorova, A. Trumpp, M. Conrad, J.P. Friedmann Angeli, 7-Dehydrocholesterol is an endogenous suppressor of ferroptosis, Nature 626 (2024) 401–410.